Int J Earth Sci (Geol Rundsch) (2009) 98:1325–1340
DOI 10.1007/s00531-008-0339-7

ORIGINAL PAPER

Magnesian andesites in north Xinjiang, China

Zhenhua Zhao · Qiang Wang · Xiaolin Xiong · Hecai Niu · Haixiang Zhang · Yulou Qiao

Received: 28 August 2007 / Accepted: 15 June 2008 / Published online: 9 August 2008

Abstract Middle Devonian magnesian andesites (MAs) are widely distributed in south Altay and Carboniferous MAs are present in Alataoshan and west- and east-Tianshan in the north Xinjiang region. These MAs are andesitic rocks with 53–65% SiO_2,<1% (0.21–1.08%; average of 0.72%) TiO_2, and ≥50 $Mg^{\#}$. Magnesian dacites and diorites, with 52.38–66.91% SiO_2, <0.30% TiO_2 and ≥42 $Mg^{\#}$ commonly occur with these MAs. Relative to boninites, MAs have lower MgO contents (average 6.39%) but higher Ti, K and Na. They have characteristic flat chondrite-normalized REE patterns with weak to no Eu anomalies (Eu depletion, or Eu/Eu* = 0.65–1.15), low $(La/Yb)_N$ (0.98–6.4, mostly 4±) and low total REE contents (15–95 ppm). They also have high contents of compatible elements Cr and Ni (72–790 and 29–276 ppm, respectively). Their relative depletion in high field strength elements Nb, Ta and Ti, and relative enrichment in mobile large-ion lithophile elements Rb, K and Pb are evident on primitive mantle-normalized trace element spidergrams. If magnesian andesites are melts coming from the subducted oceanic crust, as proposed elsewhere, then the relatively high *Y* contents (>15 ppm), low Sr/Y ratios (4.4–6.2), low (La/Yb)N, and high $Mg^{\#}$ of the MAs in north Xinjiang provide evidence of interaction of such melts with mantle wedge peridotite. New petrographic, chemical and isotopic [$(^{143}Nd/^{144}Nd)I = 0.51221–0.51255$ ($\varepsilon Nd(t)$ +0.28 to +7.2); $(^{87}Sr/^{86}Sr)I = 0.7029–0.7065$] data suggest that the petrogenesis of the MAs in the north Xinjiang region may have involved: (1) multiple source materials including subducted oceanic slab, juvenile crustal materials (mainly volcanic-volcanoclassic rocks with low maturity and clear mantle geochemical signatures) coming from the forearc accretionary prism and mantle wedge peridotite; (2) a combination of different petrogenetic processes including partial melting of subducted oceanic slab and juvenile crustal materials, followed by interaction of slab melts with the mantle wedge peridotite; (3) high geothermal gradient creating a high temperature (>1,000°C) environment in a volatile-rich source region; (4) unique tectonic settings including oblique subduction, slab break off resulting in slab window formation and asthenosphere upwelling, and subduction erosion resulting in transfer of forearc accretionary materials into the source region of MA magma.

Keywords Magnesian andesites · Metasomatism of slab melts · Subduction erosion · Asthenosphere window · North Xinjiang

Z. Zhao (✉) · X. Xiong · H. Niu · H. Zhang · Y. Qiao
Key Laboratory of Metallogenic Dynamics,
Guangzhou Institute of Geochemistry,
Chinese Academy of Sciences, 510640 Guangzhou, China
e-mail: zhzhao@gig.ac.cn

Q. Wang
Key Laboratory of Isotope Geochronology and Geochemistry,
Guangzhou Institute of Geochemistry,
Chinese Academy of Sciences, 510640 Guangzhou, China

Introduction

Magnesian andesites (MAs) or high magnesian andesites (HMAs) are important rock types in many volcanic arcs and have attracted considerable attention. They are relatively primitive in composition and represent near-primary magma in equilibrium with the mantle (Tatsumi 2006). Their origin has been attributed to partial melting of subducting slab generally followed by slab melt-mantle

interaction (Kay 1978; Kelemen 1995; Kelemen et al. 2003; Tatsumi 2006) or partial melting of strongly hydrated mantle wedge peridotites (Rapp et al. 1999; Grove et al. 2002). A new evidence that the MAs formation involved mixing of dacitic and basaltic magma and entrainment of ultramafic crystal material has provided (Streck et al. 2007). Accordingly, they are probes that provide insights into mantle melting processes, interaction between asthenosphere and lithosphere, and the nature of the crust-mantle boundary. Close compositional similarities between HMAs and bulk continental crust also suggest links between the tectonic setting of continental crustal generation and that of HMAs (Kelemen 1995; Rudnick et al. 1995; Taylor and McLennan 1995; Polat and Kerrich 2001; Tatsumi 2006). Magnesian andesites, dacites and diorites are widespread in north Xinjiang. They have been referred to mainly as HMAs or boninites in the literature (Zhang et al. 2003; Niu et al. 2006a; Wang et al. 2006). High-Mg andesites contain clinoenstatite and are characterized chemically by having 52–63% SiO_2, >8% MgO and <0.5% TiO_2 (Kikuchi 1889; Le Maitre 2002). On the other hand, Crawford et al. (1989) defined volcanic suites with >53% SiO_2 and >60 $Mg^{\#}$ [$Mg^{\#} = 100 \times Mg^{2+}/(Mg^{2+}+TFe)$] as boninites. Jenner (1981) proposed to use the term HMA separately from boninite to avoid the confusion between some ophiolite basalts and some HMAs implied by the definition of boninite. However, the criteria for HMA differ among authors. As defined by Jenner (1981), HMAs have MgO contents of ~11–20% and SiO_2 contents of 57–58% on a volatile-free basis. Kelemen (1995), on the other hand, defined HMA as an andesitic lava with >30 $Mg^{\#}$ and <10% MgO; this was later revised to >50 $Mg^{\#}$ and >54% SiO_2 (Kelemen et al. 2003). Polat and Kerrich (2001) defined HMAs as volcanic rocks with $Mg^{\#} = 50–64$ and $SiO_2 = 56–64\%$, whereas Tatsumi (2006) proposed that HMAs are andesites having FeOT/MgO <1. A SiO_2 versus MgO discrimination plot published by McCarro and Smellie (1998) distinguishes HMAs from normal volcanic rocks as volcanic rocks having $MgO = 2.8–6.5\%$ and $SiO_2 = 52–60\%$. Archean and early Paleozoic siliceous high-Mg basalts (SHMB) with 10–16% MgO and 51–55% SiO_2 were reported by Sun and McDonough (1989). Finally, igneous rocks with HMA-like chemical and petrographic features have been named after their localities, such as bajaite (Rogers and Saunderst 1989), Adak-type MA and Piip-type MA (Yogodzinski et al. 1995).

In this paper, MAs refer to high-Mg and high $Mg^{\#}$ andesitic rocks having 53–65% SiO_2, <1% (0.21–1.08%; average of 0.72%) TiO_2, and ≥50 $Mg^{\#}$. The term also generally includes some magnesian dacites and diorites, with 52.38–66.91% SiO_2, <1% TiO_2 and ≥42 $Mg^{\#}$ that commonly occur with the MAs.

Regional geology and distribution of late Paleozoic MAs in north Xinjiang

The north Xinjiang region is part of the Central Asia Orogenic Belt (CAOB) and includes multiple tectonic terranes, such as Altay, east- and west-Junggar and east- and west-Tianshan (Fig. 1). Both lateral accretion of arc complexes and vertical accretion of underplated mantle-derived materials are evident from island arc volcanic rocks, Neoproterozoic to late Paleozoic ophiolites and Paleozoic alkali-rich granites with positive εNd values (Zhao et al. 1993, 1996, 2006a; Jahn et al. 2000, 2004; Han et al. 1997, 2006; Gao et al. 2006; Niu et al. 2006a). The tectonic framework and evolution of north Xinjiang remains the subject of debate, including the issue of whether it is composed of Phanerozoic accretionary orogenic belts or terranes (Xiao et al. 2006), or Neoproterozoic basements inlaid in Phanerozoic orogenic belts (Li et al. 2004). The Paleozoic Altay continental fold belt is an accretionary belt along the southern margin of the Siberia plate. Paleozoic metamorphic clastic and clastic rocks formations are widely distributed in the area. The Junggar basin is a Mesozoic-Cenozoic terrestrial basin, which is covered by Mesozoic and Cenozoic sedimentary rocks. The nature of the basement remains uncertain. The Tianshan Mountains of north Xinjiang are composed of island arcs and microplates separated by paleo-ocean basins that opened in the Sinian and closed in Late Paleozoic. Using the Ulumqi-Korla line as the boundary, the Tianshan Mountains can be divided into west- and east-Tianshan. The Yili microplate is located in the west-Tianshan and is mainly composed of Middle- and Neo-Proterozoic metamorphic rocks, such as metamorphic sandstone, marble and slates. A Late Paleozoic fold belt or island arc is present in the northern part of the Yili microplate and a collisional orogenic belt is present in the southern part (Gao et al. 2006). The Turfan-Hami terrene (Tu-Ha basin) crops out in the east-Tianshan where Mesozoic and Cenozoic terrestrial sedimentary rocks overly a basement mainly composed of Precambrian rocks. The northern part of the Tu-Ha basin may have been a passive margin during the Silurian-Carboniferous period (Li et al. 2006) and the southern part corresponds to a late Paleozoic active margin—the east-Tianshan island arc.

Late Paleozoic MAs are widespread, in north Xinjiang at localities such as south Fuyun of Altay Mountains and Alataoshan, Dalabute, Axi and Guozigou of west-Tianshan. High-Mg dacites are mainly recognized around Ashele in the Altay Mountains and high-Mg diorites occur in the Tuwu-Yandong and Weiya areas of east-Tianshan (Fig. 1). It is worth noting that the outcrops of high-Mg igneous rocks are fairly concentrated in some areas, such as the middle Devonian MAs that occur with coeval picrites

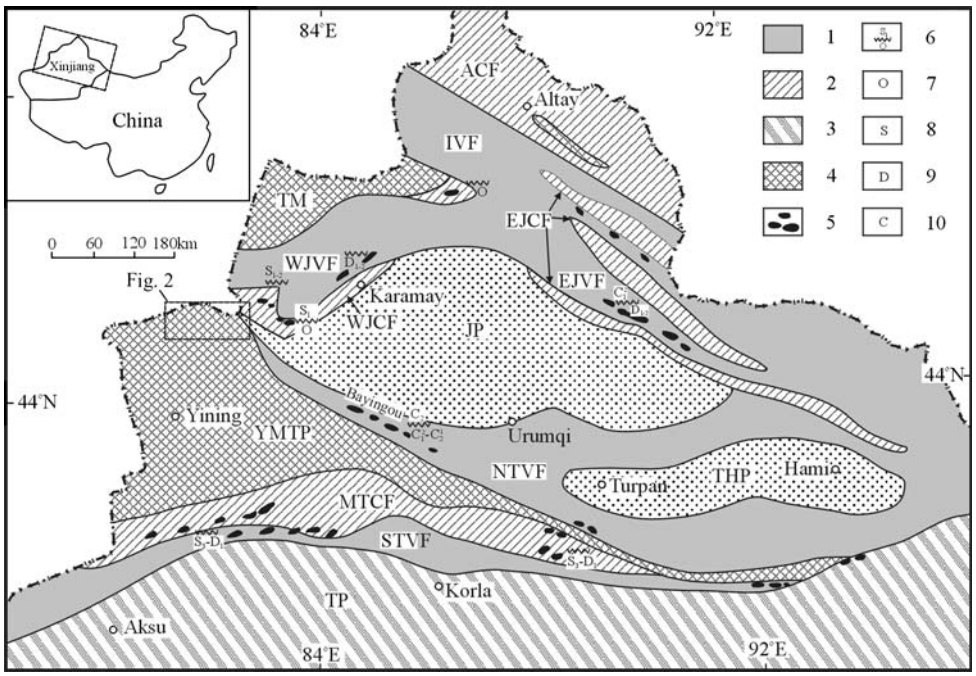

Fig. 1 Sketch map of tectonic units and the distribution of late Paleozoic magnesian igneous rocks in north Xinjiang (after Xiao et al. 1992 with some revisions) **a** late Paleozoic fold belts; **b** Early-middle Paleozoic fold belts; **c** Early Proterozoic basements; **d** LateProterozoic basements; **e** Ophiolitic fragments; **f** Cenozoic sediments; **g** formation and emplacement of ophiolite; **h** Ordovician; **i** Siliurian; **j** Devonian; **k** Carboniferous; **l** location of MAs (1. Awulale; 2. Tuwu-Yandong; 3. South Qinghe-Fuyun; 4. Luliang rise; 5. Baogutu; 6. Alataoshan; 7. Guozigou; 8.Axi); **a**, **b**: The concentrated distribution area of magnesian igneous rocks; *IPF* irtysh paleozoic fold belt, *TM* tacheng massif, *WJPF* west-junggar paleozoic fold belt; *EJPF* east-junggar fold belt, *JP* Junggar plate, *THT* tulufan-hami terrene, *NTPF* northern tianshan late paleozoic fold belt, *YMTT* yili-middle tianshan terrene, *STLPF* Southern Tianshan late Paleozoic fold belt, *STPF* southern tianshan paleozoic fold belt, *TP* Tarim plate

and late Carboniferous—early Permian mafic-ultramafic plutons in the southern Fuyun county (Fig. 1a) (Chen et al. 2004; Zhang et al. 2005). Similarly, in east Tianshan, middle-late Carboniferous MAs, high-Mg diorites, adakites and mafic-ultramafic igneous rocks are concentrated in the area of Tuwu-Yandong, Huangshan and Jing'erquan (Fig. 1b). In addition, the origins of strong mineralization of Cu, Ni, Au and Pb, Zn have been proposed to be related or partially related to these high-magnesian igneous rocks in north Xinjiang (Chen et al. 1996; Niu et al. 2006a; Wang et al. 2006). Most of them are large- or giant-scale deposits, such as the large scale Ashele Cu and Zn ore deposit, Axi Au ore deposit and Tuwu-Yandong Cu ore deposits.

Analytical methods

Major element concentrations of the majority of the samples (Ashele, Sarbulake, Axi and Alatao) were analyzed by X-ray fluorescence spectrometry (XRF) at Yamaguchi University, Japan and Hubei Institute of Geology and Mineral Resources, China. The analytical method and precisions of the XRF method were reported in Nagao et al. (1997) and Gao et al. (1995).The Dabate and Gozigou MAs were analyzed using conventional wet chemical techniques, the wet chemical techniques were reported by Gao et al. (1995). The trace elements, including rare earth elements (REE), were determined by Perkin-Elmer Sciex ELAN 6000 inductively coupled plasma mass spectrometer (ICP–MS) at the Guangzhou Institute of Geochemistry, Chinese Academy of Sciences. About 50 mg of sample powder was dissolved in high-pressure teflon bomb using a $HF + HNO_3$ mixture. An internal standard solution containing the element Rh was used to monitor the signal drift counting. The USGS standards BCR-1 and BHVO-1 were chosen for calibrating element concentrations in measured samples. The analytical precision for most elements was generally better than 5% (Liu et al. 1996). The major chemical compositions of augite phenocrysts in the MAs were determined by electron microprobe (JEOL JXA8800) at the key laboratory for mineral deposit research in Nanjing University. Operating conditions were 15 kv at 10 nA beam current. Isotopic analyses of Sr and Nd were performed on MAT-262 and multi collector (MC)-ICP–MS at the Institute of Geology and Geophysics and the Guangzhou Institute of Geochemistry, Chinese Academy of Sciences. Measured 87Sr/86Sr and 143Nd/144Nd ratios were normalized to 87Sr/86Sr = 0.1194 and 143Nd/144Nd = 0.7219,

respectively. The 87Sr/86Sr ratio of standard NBS987 and 143Nd/144Nd ratio of the La Jolla standard measured during this study were 0.710246 ± 9 (2σ) and 0.511854 ± 8 (2σ), respectively. Procedural blanks were <100 pg for Nd and <1 ng for Sr. The analytical procedures used are similar to those described by Zhang et al. (2002) and Liang et al. (2003).

Results

Petrography

The MAs of Sarbulake in south Fuyun possess amygdaloidal structure being fumaroles and vitrophyric texture. Phenocryst minerals include clinopyroxene, olivine, pseudomorphic uralite and platy plagioclase. Olivine is completely altered to serpentine minerals and shows idiomorphic crystal outlines, ranging in size from 0.2 to 1 mm long. Augite is 0.3 mm long and mostly altered to chlorite and uralite. Chromian spinel (0.1–0.3 mm) is often included in augite phenocrysts. The groundmass consists of hornblende, plagioclase and glass. The high-Mg dacites of Ashele are similar to MAs of Sarbulake, their main difference is the presence of quartz asphenocrysts in the dacites. The Axi MAs are porphyritic with plagioclase, hornblende, augite, olivine, and lesser quartz as the main phenocryst minerals. The groundmass shows semicrystalline-cryptocrystalline and hyaline crystalline texture.

The Mg/(Mg + Fe) ratios of augites cores range from 0.90–0.93 and Cr_2O_3 contents range from 0.5 to 0.7% with TiO_2 <0.1% for the Shaerbulake MAs. Chromian spinel included in an augite phenocryst has higher Cr/(Cr + Al) ratios(0.82–0.84) compared to those in boninite from Bonin islands and similar to those of mantle clinopyroxene (Table 1; Niu et al. 2006a). Augites of the Guozigou and Alataoshan MAs have Mg/(Mg + Fe) = 0.77, 0.82 and Cr2O3 = 0.14%, 0.37% respectively (Table 1). These features together with their low FeOT/MgO ratios suggest the presence of high-Mg magma (Tatsumi 2006).

Major element chemistry

Chemically, the MAs are mainly basaltic andesite and andesite and lesser amounts of dacite and diorite in the study area (Table 2). They are the low-Ca type of MAs based on their low CaO/Al_2O_3 = 0.10–0.49 (Crawford et al. 1989), SiO_2 = 53–65%, MgO = 3.12–12.19% (average 6.39%), $Mg^{\#} \geq 51$ and $TiO_2 < 1.0\%$. The MAs are rich in alkalis with $K_2O > 1\%$ and $Na_2O > 2\%$. Compared with the global average composition of boninites (Table 2, 334 samples, Kelemen et al. 2003), the MAs of north Xinjiang are characterized by relatively lower MgO contents, higher TiO_2 and higher FeOT/MgO ratios. The Ashele high-Mg dacites have low MgO concentrations (2.69–5.24%), $Mg^{\#}$ = 42–57 and FeOT/MgO > 1 (1.11–1.85, average 1.47). All the MAs of north Xinjiang plot in the MA field in the SiO_2 versus MgO diagram of McCarro and Smellie (1998) (Fig. 2). In addition, the experimental data on natural, hydrous basalts at 1–4 Gpa are plotted in the Fig. 2, it is evident that the $Mg^{\#}$ of "pure slab melts" are not confident with that of MAs (Rapp et al. 1999).

Table 1 Compositions of clinopyroxene (Cp) and spinele (Sp) from north Xinjiang MAs (%)

Mineral	Cp	Cp	Cp	Sp	Sp	Cp	Cp
Sample no	As1	As2	As3	As4	As5	Xt28	Xt358
SiO_2	55.22	54.97	54.33	0.00	0.06	55.39	52.71
TiO_2	0.04	0.02	0.05	0.15	0.23	0.39	0.67
Al_2O_3	0.53	0.68	1.16	7.14	7.31	2.69	4.10
Cr_2O_3	0.54	0.60	0.63	56.4	54.68	0.37	0.14
FeO	2.55	2.93	3.75	27.5	28.97	6.87	8.95
MnO	0.14	0.07	0.12	0.63	0.7	0.19	0.15
NiO	0.04	0.05	0.00	0.05	0.07	0.04	0.00
MgO	19.01	18.37	18.59	7.83	7.97	17.29	16.83
CaO	22.85	22.75	21.99	0.03	0.04	17.85	17.60
Na_2O	0.07	0.13	0.13	0.03	0.02	0.22	0.31
K_2O	0.02	0	0.04	0.03	0.01	0.02	0.00
Σ	100.98	100.58	100.78	100.78	100.06	101.32	101.46
Mg/(Mg + Fe)	0.93	0.92	0.90	0.40	0.41	0.82	0.77
Cr/(Cr + Al)	0.41	0.37	0.27	0.84	0.83	0.009	0.0022

As1-5 Ashele, *Xt28* Alataoshan, *Xt358* Guozigou

Trace element chemistry

The total REE concentrations range from 15 to 95 ppm, but typically about 50 ppm. The samples are slightly depleted to enriched in light rare earth elements. (LREE) relative to the heavy.rare earth elements (HREE) [$(La/Yb)N$ = 0.98–6.4, mostly have ~4], and show in flat or convex upward chondrite-normalized REE patterns (Fig. 3). Europium shows no- or weak depletions, with Eu/Eu* = 0.62–1.15 (Table 2). The relationship between $(Dy/Yb)_N$ and $(La/Yb)_N$ for north Xinjiang MAs is shown in Fig. 4. Low$(Dy/Yb)_N$ (<1.5) and relatively high $(La/Yb)_N$ (>1.39) are clear comparing with that of primitive mantle (Sun and McDonough 1989).

The MAs of north Xinjiang are characterized by high concentrations of compatible elements, such as Cr and Ni (72–790 and 29–276 ppm, respectively). The highest contents of Cr and Ni are 467–1,112 and 171–276 ppm, respectively, in the Axi MAs (Table 2). The high field strength elements (HFSE) Nb, Ta and Ti are depleted

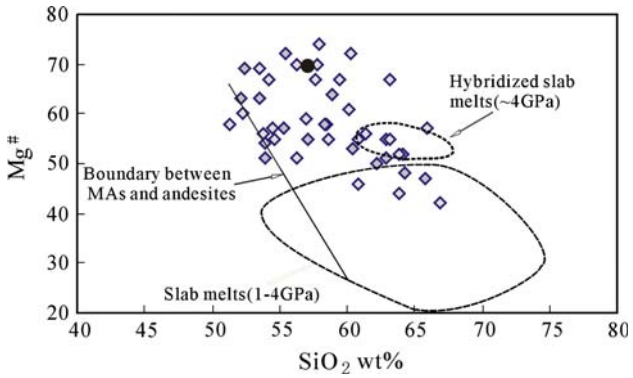

Fig. 2 Diagram of SiO_2 versus MgO for MAs in north Xinjiang Solid circle: world average boninite (Kelemen et al. 2003); The boundary line between MAs and normal andesites (McCarro and Smellie 1998); the slab melts at 1–4 GPa and hybradized slab melts at ~4 GPa (Rapp et al. 1999)

relative to other incompatible trace elements, resulting in distinctly negative anomalies on primitive-mantle normalized spidergrams (Fig. 5). In contrast, the large-ion-lithophile (LIL) elements, such as Rb and K, are relatively enriched. Wide ranges of Sr/Y ratio (4.4–62) and high concentrations of Y (>15 ppm) result in samples plotting in the transitional area between island arc andesites- dacites and adakites on a Sr/Y versus Y diagram (Fig. 6).

High Th/Yb ratios in arc lavas are indicative of the involvement of sediments and/or sediments-derived melts in their generation (Woodhead et al. 2001). On the other hand, Ba is a fluid-mobile alkaline earth element (AEE) and fractionation of AEE with respect to REE, such as high Ba/La, is believed to reflect the involvement of hydrous fluids in arc magma generation (Woodhead et al. 2001). The MAs of north Xinjiang are characterized by very low. Th/Yb ratios (0.18–3.32) yet display a wide range and relatively high Ba/La ratios (5.4–816). These MAs plot parallel with the Ba/La axis in the Th/Yb versus Ba/La diagram (Fig. 7), and this suggests input of hydrous fluids and only minor contribution of sedimentary materials in their generation.

Chronology

Different isotopic dating methods were employed to the MAs of north Xinjiang. The dating results, together with the presence of fossils, show the MAs were mainly generated in the middle Devonian and Carboniferous. In the Saerbulake area, South Fuyun county of east Altay, the MAs occur mainly in the Beitashan group of middle Devonian age based on the presence of fossils Leptostrophia sp., Elytha sp., Xinjiangolites sp. and Prismatophyllum xinjiangense, etc. (Liu et al. 1993). The high-Mg dacites are distributed throughout the Ashele group of lower-middle Devonian in west Altay (Chen et al. 1996). Isotopic dating by the Sm–Nd and Rb–Sr methods for jaspilite in this group gave ages of 372 ± 14 and 378 ± 39 Ma, respectively; the Sm–Nd isochron age of the Qiye group overlying the Ashele group is 359.9 ± 11 Ma (Li et al. 1998). Thus isotopic data together with paleontologic data suggest the high-Mg dacites in the Ashele area were generated during middle-early Devonian.

$^{40}Ar/^{39}Ar$ dating yields an isochron age of 332.70 ± 6.65 Ma for MA in the Bayingou ophiolite in the west-Tianshan late Paleozoic folt belt (Wang et al. 2006). The ages of plagioclase granite and gabbro in the ophiolite are 324.7 Ma (SHRIMP zircon U–Pb age) and 342.6 ± 2.2 Ma (zircon U–Pb age, LA-ICPMS), respectively (Xu et al. 2005, 2006). Tectonicly, the Alataoshan volcanic

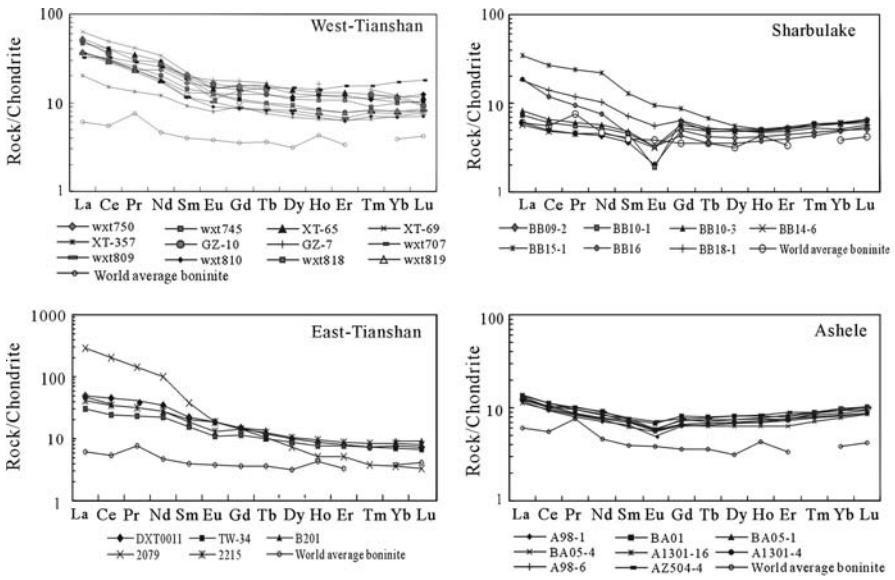

Fig. 3 Chondrite-normalized REE patterns for MAs in north Xinjiang

Table 2 Major (wt%),trace and REE (μg/g) compositions of representative samples for the magnesian igneous rocks in north Xinjiang

Location	Alataoshan				Dabate		Guozjgou				Axi						Bayingou	Tuwu-yandong		Qi'ershan		
Type	MAs																					
Sample no.	wxt 750	Xt -28	wxt 745	Xt -27	XT65	XT69	XT 357	XT 358	GZ10	GZ7	wxt 809	wxt810	wxt 818	wxt 819	Xa24	Xa29	wxt 707	DXT 0011	TW34	B201	D98 -1	D146 -1
SiO_2	57.04	61.44	56.99	59.43	62.9	63.13	52.28	58.48	55.29	54.53	55.41	60.32	57.93	56.23	60.87	53.57	63.17	53.97	51.35	57.63	60.12	53.84
TiO_2	1.01	0.74	0.94	0.64	0.79	0.64	0.38	0.98	0.96	0.96	0.77	0.6	0.72	0.74	0.76	0.86	0.76	0.94	1.03	0.97	0.61	0.98
Al_2O_3	16.32	15.20	14.89	15.95	15.47	15	16.06	14.89	14.85	14.84	14.59	12.3	15.19	15.26	16.03	13.6	14.33	16.94	18.38	14.64	14.57	17.70
Fe_2O_3	2.25	3.03	2.39	3.91	1.27	2.32	2.04	2.66	3.02	4.27	7.54	6.29	5.36	7.26	2.71	4.41	1.46	7.55	2.52	2.35	2.03	3.66
FeO	4.65	1.57	3.37	0.57	4.08	2.48	5.19	4.85	4.78	4.07	ND	ND	ND	ND	2.55	4.23	3.8	ND	6.45	3.95	4.11	4.13
MnO	0.08	0.08	0.06	0.08	0.02	0.04	0.16	0.12	0.12	0.14	0.07	0.08	0.06	0.07	0.11	0.1	0.06	0.14	0.07	0.11	0.16	0.17
MgO	4.66	3.05	4.52	3.96	3.6	3.12	5.81	5.6	5.5	5.7	9.72	8.05	7.65	8.47	4.05	8.01	5.92	4.54	6.67	6.8	5.21	5.27
CaO	6.8	6.19	4.69	3.99	1.59	3.87	7.39	4.06	4.82	6.47	2.18	3.13	4.9	4.38	5.59	3.84	2.16	6.76	4.42	5	7.49	6.35
Na_2O	2.41	3.80	2.54	4.83	4.5	4.16	1.61	3.66	3.8	4.84	2.57	1.65	2.54	2.65	3.68	1.77	3.67	4.56	3.21	3.9	3.24	2.89
K_2O	0.87	1.73	2.62	1.40	2.97	2.1	2.4	1.51	1.37	0.24	0.72	0.98	1.76	1.45	1.37	0.22	0.56	0.07	0.41	1.8	0.06	0.38
P_2O_5	0.12	0.42	0.15	0.36	0.15	0.36	0.34	0.11	0.14	0.15	0.09	0.08	0.08	0.06	0.01	0.01	0.11	0.26	0.29	0.23	0.12	0.31
H_2O	1.00	2.36	3.89	3.07	2.11	3.33		2.78									0.04		4.78		2.60	4.00
LOI				1.2			5.83		3.63	3.94	6.42	6.7	3.36	3.92	2.31	9.47		4.79		2.22		
Σ	99.8	99.61	99.8	99.52	99.45	100.55	93.66	99.72	98.28	100.09	93.67	93.46	96.2	96.57	100.04	100.09	99.77	95.73	99.73	97.38	100.96	99.8
$Mg^{\#}$	55	56	59	67	55	55	60	58	57	57	72	72	74	70	55	63	67	54	58	67	61	56
Sc	24.7	17	16.6	17	19	15	42.9	24.6	ND	ND	20.4	13	17	15.3	17	16	14.3	ND	ND	ND	21	25
V	158	108	107	121	72	98	299	193	276	305	120	99.4	117	118	117	161	110	ND	ND	ND	132	187
Cr	253	39	254	445	72	73	79.1	148	168	162	1132	467	790	768	140	15	13.8	ND	ND	ND	283	73
Co	24.3	17	24.9	17	8	16	25.6	22.2	29.5	30.6	33.1	24.9	26.6	27.2	19	95	7.85	27.4	ND	ND	16	26
Ni	76.2	22	161	22	43	40	29	28	ND	ND	276	171	182	183	58	97	8.09	45.6	ND	ND	90	50
Ga	19.1	17	17.9	18	19	20	14.2	17.6	ND	ND	14	12.9	16.1	16.1	ND	ND	16.3	ND	ND	ND	16	22
Rb	20.8	43	73.2	34	286	71	56.1	27.0	28.6	42.3	36.4	53.8	59.4	29.5	57	42	26.7	2.41	ND	29.1	0.7	6.8
Sr	265	512	225	432	349	421	537	546	856	1007	81.7	64.1	297	294	346	217	139	1666	ND	260	434	839
Y	23.2	16	21.5	17	28	27	12.4	16.4	9.0	8.0	15	14.5	17.4	17.2	14	20	22.6	16.7	15.3	18.1	13.5	15.1
Zr	173	125	175	129	156	156	31.4	140	111	83	105	88.3	128	114	87	91	165	120	ND	165	111	142
Nb	6.92	4.0	7.3	5.0	8.0	7.0	1.24	6.3	9.0	8.0	4.34	4.59	6.02	5.74	26	25	4.29	2.86	ND	5.7	3.1	5.8
Ba	376	427	270	541	356	342	654	927	525	145	59.4	74.7	295	287	300	614	862	298	ND	374	55	234
Hf	4.17	2.90	4.16	3.05	3.98	3.91	0.65	3.62	3.64	3.67	2.71	2.39	3.58	3.08	3.41	6.3	5.13	2.97	ND	2.98	2.80	3.6
Ta	0.57	0.35	0.63	0.37	0.56	0.52	0.14	0.46	9.56	050	0.36	0.38	0.54	0.47	0.55	0.53	0.38	0.22	ND	ND	0.20	2.4
Pb	8.52	ND	14.7		ND	ND	7.51	5.22	ND	ND	8.9	9.66	12.2	11.4	ND	ND	7.08	ND	ND	ND	6.2	7.1
Th	4.99	3.33	6.79	3.55	6.66	6.9	1.64	4.28	3.85	3.82	3.18	4.13	5.5	5.11	5.62	5.73	4.26	2.08	ND	3.22	4.0	1.8
U	1.57	1.03	1.95	0.99	1.37	1.48	0.69	1.00	1.21	1.28	0.90	1.12	1.58	1.37	1.62	1.02	1.29	ND	ND	ND	1.0	0.6
La	11.2	13.31	14.3	13.62	16.23	19.6	6.26	11.7	15.7	15.3	10.9	11.6	11.3	11.5	15.2	21.4	9.96	15.2	9.33	14.9	10.36	16.65
Ce	24.7	26.22	32.3	27.48	32.6	39.7	12.2	24.4	28.4	29.5	22.9	24.2	24.8	23.4	30.5	46.1	26.1	37	19.8	28.6	21.53	37.34
Pr	2.86	3.28	3.67	3.37	4.25	4.98	1.62	3.22	ND	ND	2.73	2.84	3.07	2.86	ND	ND	3.51	4.95	2.86	ND	2.37	4.08
Nd	14	13.17	17	13.73	17.4	20.2	7.28	13.4	15.7	15.4	10.3	10.6	12.2	11.1	14.9	20.3	15.2	20.3	13.1	16.9	11.49	19.21
Sm	3.24	2.73	3.68	2.8	3.87	4.27	1.77	2.99	3.89	3.8	2.21	2.23	2.77	2.52	3.09	4.38	3.59	4.26	3.10	4.00	2.78	3.81

Table 2 continued

Location	Alataoshan				Dabate		Guozjgou				Axi						Bayingou	Tuwu-yandong		Qi'ershan		
Type	MAs																					
Sample no.	wxt 750	Xt -28	wxt 745	Xt -27	XT65	XT69	XT 357	XT 358	GZ10	GZ7	wxt 809	wxt810	wxt 818	wxt 819	Xa24	Xa29	wxt 707	DXT 0011	TW34	B201	D98 -1	D146 -1
Eu	1.11	0.85	0.94	0.88	1.04	1.04	0.58	0.99	1.19	1.32	0.75	0.66	0.93	0.93	1.03	1.26	0.79	1.35	0.82	1.35	0.82	1.37
Gd	3.58	2.66	3.18	2.77	4.01	4.13	2.29	3.09	3.89	4.55	2.27	2.18	2.85	2.67	3.76	4.87	3.56	3.78	3.02	3.93	3.88	4.45
Tb	0.59	0.45	0.59	0.46	0.74	0.71	0.35	0.53	0.67	0.80	0.40	0.38	0.47	0.46	0.57	0.84	0.70	0.57	0.47	0.64	0.42	0.56
Dy	3.69	2.52	3.5	2.63	4.44	4.09	2.21	3.08	ND	ND	2.6	2.4	3.02	2.84	ND	ND	4.76	3.18	2.83	ND	2.79	2.98
Ho	0.86	0.53	0.76	0.54	0.94	0.86	0.47	0.62	0.98	1.17	0.52	0.49	0.60	0.59	nd	nd	1.01	0.62	0.56	nd	0.56	0.63
Er	2.54	1.52	2.25	1.53	2.71	2.40	1.34	1.71	ND	ND	1.41	1.29	1.62	1.64	ND	ND	3.25	1.67	1.61	ND	1.55	1.59
Tm	0.35	0.21	0.29	0.22	0.4	0.35	0.21	0.278	0.40	0.45	0.25	0.23	0.27	0.26	ND	ND	0.50	0.24	0.24	ND	0.23	0.24
Yb	2.37	1.35	2.06	1.40	2.47	2.14	1.45	1.83	2.35	2.51	1.56	1.41	1.66	1.69	1.77	3.30	3.56	1.60	1.47	1.91	1.47	1.59
Lu	0.41	0.21	0.35	0.22	0.38	0.34	0.25	0.30	0.31	0.32	0.27	0.23	0.28	0.26	0.27	0.51	0.60	0.24	0.22	0.30	0.26	0.27
ΣREE	71.50	69.02	84.85	71.65	91.48	104.81	38.29	68.13	73.47	75.11	59.07	60.74	65.84	62.72	71.09	103.0	77.09	94.96	59.43	72.53	60.57	94.77
$(La/Yb)_N$	3.17	6.65	4.65	6.54	4.40	6.14	2.89	4.28	4.48	4.08	4.68	5.51	4.56	4.56	5.75	4.34	1.87	6.37	4.25	5.23	4.72	7.02
Eu/Eu*	1.00	0.97	0.84	0.97	0.81	0.76	0.88	0.99	0.94	0.97	1.02	0.91	1.01	1.10	0.92	0.83	0.68	1.03	0.82	1.04	0.76	1.02

Location	Road No312	North Beiya	World boninite[1]	Saerbulake							Ashele												
Type	MDs	MDs	MDs	MAs							Magnesian dacite												
Sample no	2,079	2215	348 samples	BB09 -2	BB10 -1	BB10 -3	BB14 -6	BB15 -1	BB16	BB18 -1	A98-1	BA01	BA05 -1	BA05 -4	A1301 -16	A1301 -4	A98 -6	AZ504 -4	AZ504 -6	AZ509 -10	AZ509 -8	A408 -19	Az509 -16
SiO_2	58.41	54.56	56.83	57.76	54.22	58.94	52.13	53.95	56.25	60.45	62.2	60.76	63.83	64.25	66.91	65.89	64.1	63.89	58.62	62.93	65.73	52.38	53.54
TiO_2	0.8	0.79	0.25	0.24	0.3	0.25	0.33	0.35	0.21	0.34	0.27	0.32	0.27	0.29	0.28	0.29	0.28	0.29	0.31	0.27	0.26	0.59	0.61
Al_2O_3	15.43	17.1	13.22	9.59	12.18	9.97	12.84	16.01	16.23	14.83	13.6	15.02	14.35	14.36	14.06	3.86	4.23	15.1	13.89	14.25	13.96	13.91	13.94
Fe_2O_3	6.68	8.33	7.93	1.11	1.92	1.74	2.65	3.83	2.92	2.06	2.54	2.38	2.15	1.54	3.24	2.34	2.01	1.82	2.1	1.02	1.06	2.52	2.30
FeO	ND	ND	ND	5.85	6.05	6.1	6.18	4.9	3.65	4.0	3.74	4.50	3.32	4..30	3.25	3.29	3.92	5.32	5.82	4.72	4.5	6.91	7.43
MnO	0.11	0.11	0.15	0.15	0.16	0.18	0.16	0.14	0.1	0.15	0.15	0.09	0.04	0.04	0.10	0.08	0.07	0.1	0.09	0.11	0.08	0.14	0.16
MgO	4.61	5.05	10.64	8.99	9.31	7.82	8.73	5.22	3.91	3.97	3.37	3.16	2.37	2.98	2.56	3.92	3.43	4.31	5.24	3.26	2.69	11.34	12.19
CaO	6	8.32	8.35	8.6	8.09	9.46	8.35	5.84	5.51	4.66	3.47	5.18	3.93	3.34	1.65	0.99	2	1.89	2.06	3.36	3.47	6.18	5.83
Na_2O	4.73	3.62	2.02	2.12	2	1.75	2.22	4.3	3.25	3.61	3.63	2.87	3.49	3.26	5.02	3.89	3.26	3.45	3.18	3.43	2.87	1.74	1.28
K_2O	1.92	0.61	0.56	2.53	2.91	1.88	2.02	2.06	3.23	2.02	0.55	0.78	0.85	1.02	0.56	1.3	1.61	0.9	0.61	1.58	1.22	0.3	0.31
P_2O_5	0.23	0.2	0.06	0.19	0.22	0.33	0.15	0.41	0.28	0.2	0.06	0.04	0.05	0.04	0.06	0.06	0.07	0.06	0.05	0.06	0.06	0.11	0.09
LOI	1.22	1.21		2.18	2.04	1.56	3.14	2.32	3.69	3.36	5.94	4.98	4.81	4.79	2.77	3.37	4.68	2.66	4.04	4.63	3.85	3.78	2.18
Σ	98.92	98.69	100.01	99.31	99.4	99.98	98.9	99.33	99.23	99.65	99.52	100.08	99.46	100.21	100.46	89.28	89.66	99.79	96.01	99.62	99.75	99.9	99.86
$Mg^{\#}$	58	55	70	70	67	64	63	51	51	53	50	46	44	48	42	57	52	52	55	51	47	69	69
Sc	ND	ND	36.45	37.1	39.8	31.4	51.5	39.9	30.7	24.3	24	33	24	25	23	24	25	19	45	35	7	33	38
V	ND	ND	188.01	201	195	189	275	250	215	168	113	151	117	122	148	133	121	134	146	125	114	218	207
Cr	ND	ND	696.03	395	266	265	385	74.9	39.2	75.7	3	10	6	14	3	2	1	9	14	26	7	265	251
Co	4.35	25.4	43.1	44.9	32.8	28.6	35.9	23.9	19.2	18.3	14	16	12	13	12	12	12	26	30	33	26	36	46

Table 2 continued

Location	Road No312	North Beiya	World boninite[1]	Saerbulake							Ashele												
Type	MDs	MDs	MDs	MAs							Magnesian dacite												
Sample no	2,079	2215	348 samples	BB09-2	BB10-1	BB10-3	BB14-6	BB15-1	BB16	BB18-1	A98-1	BA01	BA05-1	BA05-4	A1301-16	A1301-4	A98-6	AZ504-4	AZ504-6	AZ509-10	AZ509-8	A408-19	Az509-16
Ni	2.28	32.9	191.76	111	105	77.2	68.8	30.8	29.2	31	3	3	2	5	3	2	2	ND	ND	ND	ND	84	ND
Ga	ND	ND	ND	ND	ND	ND	ND	ND	ND	ND	ND	ND	ND	ND	ND	ND	ND	ND	ND	ND	ND	ND	ND
Rb	163	16.7	9.47	30.2	45.2	28.5	20.9	24.9	44.9	22	ND	ND	ND	ND	ND	ND	ND	ND	ND	ND	ND	ND	ND
Sr	488	543	141.84	131	300	242	170	685	791	597	118	119	144	101	116	76	83	83	82	82	70	67	22
Y	9.82	18.7	7.59	9.06	10.9	12.2	10.7	11.1	8.1	10.2	14	16	15	13	16	14	15	13	12	10	11	10	10
Zr	315	48.9	39.05	13.3	17.2	14.1	15.8	17.3	12.5	27.4	39	41	40	38	43	43							
Nb	11.4	2.84	2.17	0.7	0.87	0.7	1.15	2.33	2.7	3.1	1	1	1	0.9	1.1	1.1	1.1	0.9	0.8	0.9	0.9	0.5	0.5
Ba	2023	187	54.53	1511	1573	732	763	562	894	651	79	94	128	116	76	122	168	96	64	134	134	661	191
Hf	8.57	1.6	0.7	0.38	0.49	0.4	0.47	0.61	0.39	0.76	1.25	1.39	1.37	1.29	1.35	1.36	1.3	1.15	1.01	1.19	1.25	0.73	0.92
Ta	0.65	0.15	0.13	0.05	0.06	0.05	0.08	0.14	0.16	0.19	0.1	0.09	0.08	0.08	0.09	0.09	0.1	0.08	0.06	0.08	0.08	0.05	0.04
Pb	ND	ND	1.83	ND	ND	ND	ND	ND	ND	ND	4	3	2	3	4	3	3	3	3	4	5	3	16
Th	22.4	2.53	0.42	0.28	0.33	0.26	0.223	1.38	0.58	0.81	1.42	1.6	1.52	1.4	1.53	1.56	1.48	0.51	1.01	0.64	0.67	0.46	0.52
U	ND	ND	0.26	0.26	0.59	0.56	0.14	0.65	0.34	0.334	0.46	0.49	0.5	0.44	0.54	0.55	0.47	0.52	0.38	0.51	0.46	0.12	0.16
La	89.9	12.7	1.88	1.85	2.27	2.53	1.79	10.7	5.74	5.65	3.63	4.17	4.04	3.44	4.28	3.69	3.78	3.93	2.51	3.7	3.65	2.71	1.4
Ce	167	28.4	4.44	4	4.83	5.3	3.94	21.3	9.66	11.4	7.48	9.02	8.36	7.64	9.11	8.48	8.06	8.26	4.85	8.03	7.17	6.61	2.94
Pr	17.3	3.86	0.92	0.55	0.67	0.74	0.56	2.88	1.14	1.44	0.98	1.23	1.16	1.02	1.16	1.07	1.05	1.24	0.83	1.13	1.11	0.98	0.56
ND	60.1	16.3	2.79	2.61	3.17	3.4	2.73	13	4.49	6.12	4.25	5.49	5.13	4.49	5.03	4.69	4.53	5.35	3.71	4.86	4.73	4.81	2.79
Sm	7.42	3.59	0.77	0.7	0.89	0.95	0.8	2.51	0.89	1.39	1.27	1.46	1.37	1.20	1.47	1.41	1.35	1.53	1.13	1.33	1.36	1.31	1.00
Eu	1.35	0.97	0.28	0.15	0.14	0.24	0.23	0.69	0.24	0.41	0.36	0.5	0.43	0.41	0.44	0.43	0.42	0.52	0.33	0.41	0.47	0.48	0.47
Gd	3.65	3.7	0.92	1.28	1.61	1.49	1.35	2.26	1.13	1.65	1.65	2.1	1.94	1.67	1.88	1.71	1.73	1.95	1.48	1.74	1.75	1.58	1.55
Tb	0.49	0.58	0.17	0.2	0.23	0.24	0.23	0.32	0.17	0.25	0.31	0.38	0.34	0.3	0.35	0.32	0.32	0.37	0.28	0.32	0.32	0.26	0.29
Dy	2.32	3.44	1.01	1.32	1.56	1.62	1.55	1.79	1.13	1.6	2.17	2.62	2.4	2.06	2.42	2.23	2.23	2.62	2.01	2.26	2.25	1.77	1.95
Ho	0.37	0.68	0.31	0.3	0.36	0.37	0.35	0.37	0.27	0.34	0.5	0.59	0.54	0.46	0.56	0.5	0.52	0.6	0.46	0.51	0.51	0.4	0.42
Er	1.07	1.81	0.70	0.92	1.07	1.14	1.06	1.09	0.82	1.00	1.52	1.67	1.55	1.32	1.74	1.58	1.6	1.89	1.45	1.61	1.67	1.18	1.29
Tm	0.12	0.27	ND	0.15	0.19	0.19	0.18	0.18	0.14	0.17	0.25	0.29	0.28	0.23	0.29	0.26	0.27	0.29	0.23	0.25	0.26	0.18	0.19
Yb	0.75	1.72	0.80	1.03	1.24	1.26	1.22	1.25	1.01	1.08	1.71	2.02	1.94	1.62	1.95	1.75	1.83	2.05	1.62	1.81	1.86	1.12	1.29
Lu	0.11	0.27	0.14	0.17	0.21	0.22	0.2	0.21	0.18	0.19	0.29	0.34	0.34	0.28	0.32	0.29	0.31	0.33	0.26	0.28	0.3	0.18	0.21
ΣREE	351.95	78.29	15.13	15.23	18.44	19.69	16.19	58.55	27.01	32.69	26.37	31.88	29.82	26.14	31.00	28.41	28	30.93	21.15	28.24	27.41	25.57	16.35
(La/Yb)N	80.31	4.95	1.57	1.2	1.23	1.34	0.98	5.74	3.81	3.51	1.42	1.38	1.4	1.42	1.47	1.41	1.38	1.28	1.04	1.37	1.31	1.62	0.73
Eu/Eu[a]	0.79	0.81	1.02	0.48	0.36	0.62	0.68	0.89	0.73	0.83	0.76	0.87	0.81	0.89	0.81	0.85	0.84	0.92	0.78	0.82	0.93	1.02	1.15

nd not determined; $Mg^{\#}$ molar100 × Mg/(Mg + Fe_{tol})

[1] After Kelemen (2003)

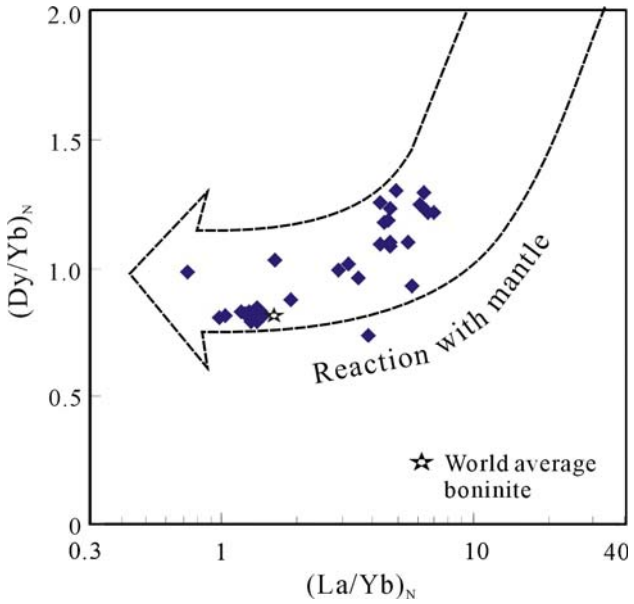

Fig. 4 Relationship between $(Dy/Yb)_N$ and $(La/Yb)_N$ for north Xinjiang MAs. *Arrow* shows the reaction of partial melts of MORB with upper mantle peridotite (Kelemen et al. 2003)

rocks including adakites, Nb-enriched basalts and MAs are distributed in the northwest of Bayingou ophiolite of the west Tianshan. $^{40}Ar/^{39}Ar$ dating on the adakites, Nb-enriched basalts and volcanic rocks in Alataoshan gave plateau ages of 320 ± 1, 319 ± 2 and 306 ± 4 Ma, respectively (Wang et al. 2006). Ages of 310–340 Ma for other volcanic rocks in this area were reported by Chen et al. (2000). Thus, the MAs spatially associated with these volcanic rocks in Alataoshan are of middle-late Carboniferous age.

Rubidium-Sr, $^{40}Ar/^{39}Ar$ and SHRIMP zircon U–Pb dating on the Axi MAs, west-Tianshan, gave ages of 346 ± 9, 325.1 ± 0.6 and 363.5 ± 5.7 Ma, respectively (Li et al. 1998; Zhai et al. 2006). We also carried out SHRIMP zircon U–Pb dating and obtained an age of about 340 Ma (Wang et al. unpublished data). Collectively, these results suggest that the Axi MAs are early-middle Carboniferous in age.

In east-Tianshan, ages of 334.3 ± 3 Ma (SHRIMP zircon U–Pb; Chen et al. 2005), 322 ± 10 and 308.5 Ma (zircon U–Pb; Liu et al. 2003) were reported for the Tuwu-Yandong adakitic granodiorite porphyry, Chihu quartz diorite and Qi'eshan quartz diorite, respectively. These data suggest these magnesian-rich, intermediate plutons were formed during middle-late Carboniferous. From the above data, it appears that the MAs become younger (from Devonian to Carboniferous) from north to south in north Xinjiang.

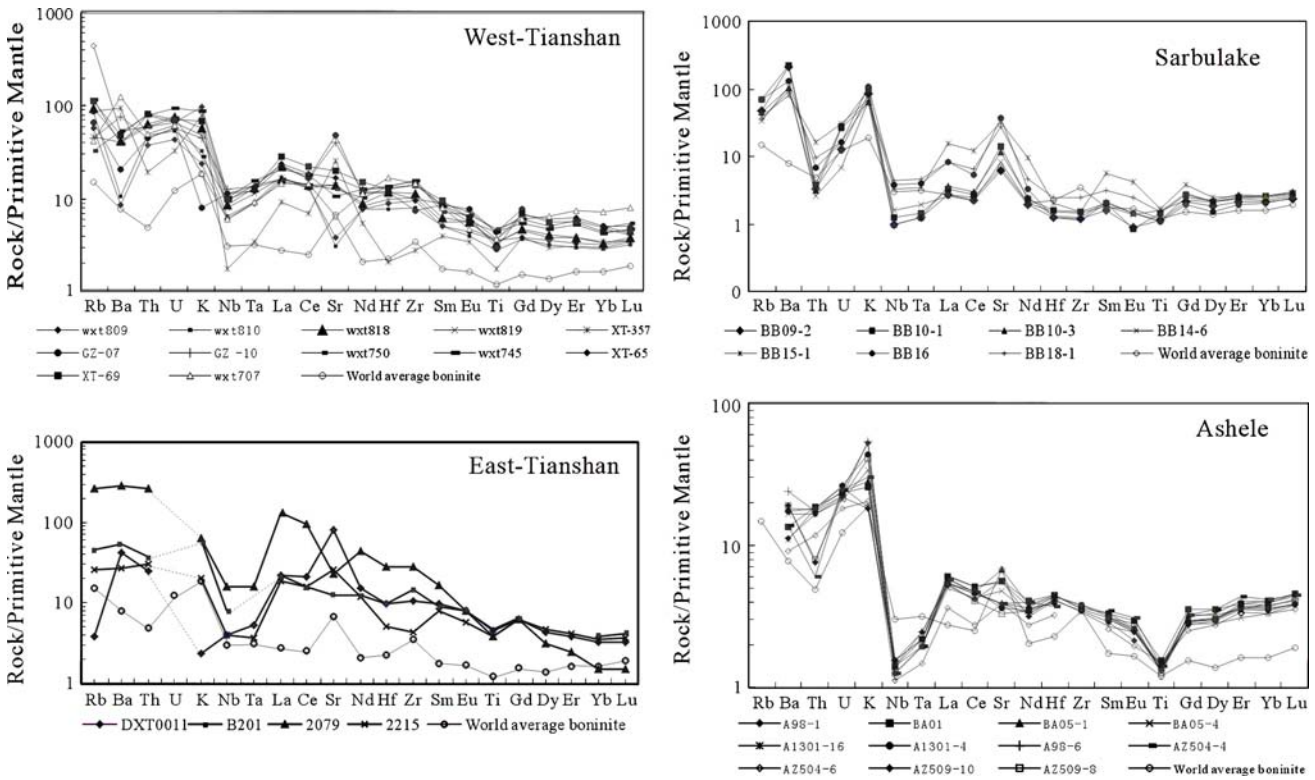

Fig. 5 Primitive mantle-normalized spidergram of trace elements for MAs in north Xinjiang (The primitive mantle values are after Sun and McDonough 1989)

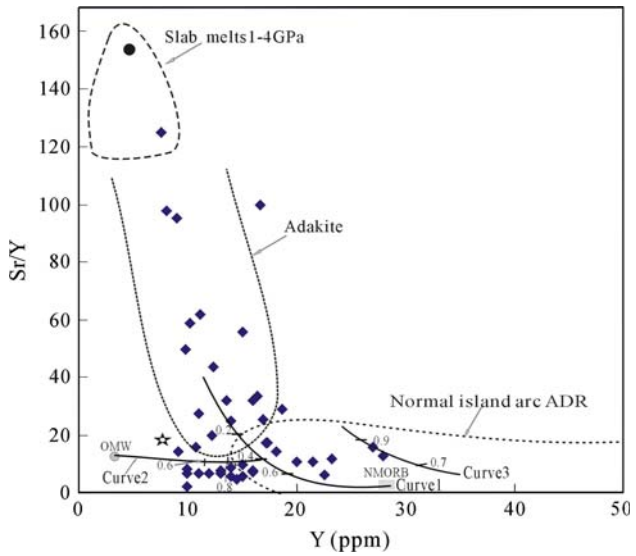

Fig. 6 Diagram of Sr/Y versus Y for MAs in north Xinjiang (Defant and Drummond 1993). Curve 1; Partial melting of NMORB under amphibolite-eclogite phase. The numbers (0.2, 0.4, 0.6) along the curve represent the proportion of amount of melts. Residual minerals: 35% clionopyroxene, 30% amphibole, 35% garnet. The partition coefficients are from Green et al. 1989; Green 1994; Adam et al. 1993; Jenner et al. 1993; Kennedy et al. 1993. The NMORB is from Sun and McDonough 1989. Curve 2: Mixing model of slab melts(40% partial melt of NMORB) with original mantle wedge (OMW)(Tatsumi and Hanyu 2003). The numbers along the curve represent the proportion of slab melts. The mixing equation is from Allegre and Minster 1977. Curve 3: Crystal-fractionation model. The numbers along the curve represent the melt remaining. Fractionating phases; 30% clinopyroxene, 30% orthopyroxene, 40% plagioclase (After Defant and Drummond 1993) Slab melts 1–4 Gpa (Rapp et al. 1999)

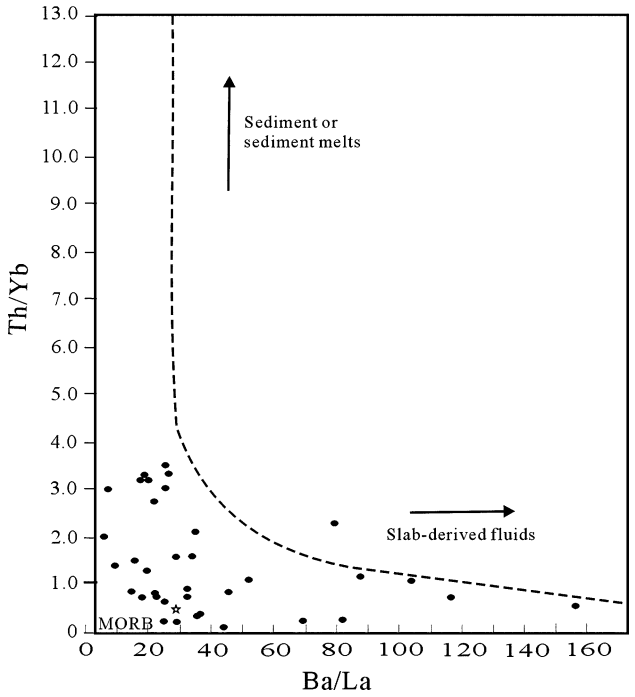

Fig. 7 Diagram of Th/Yb versus Ba/La for MAs in north Xinjiang (Woodhead et al. 2001)

Sr and Nd isotopic geochemistry

The north Xinjiang MAs possess a wide range of initial $^{87}Sr/^{86}Sr$ ratios (0.7029–0.7065) and 143Nd/144 ratios (0.51227–0.51255; $\varepsilon Nd(t)$ =+0.28 to +7.2 and Nd model ages(T2DM) of 707–1,220 Ma) (Table 3). In comparison with average boninite (Kelemen et al. 2003), the north Xinjiang MAs have lower ($^{143}Nd/^{144}Nd$)i and higher ($^{87}Sr/^{86}Sr$)I ratios. In an $\varepsilon Nd(t)$ versus ($^{87}Sr/^{86}Sr$)i diagram, the MAs mostly plot in the high $\varepsilon Nd(t)$ and ($^{87}Sr/^{86}Sr$) quadrant and trend parallel to the mantle array (Fig. 8). Differences between the MAs and the late Paleozoic adakites and Nb-enriched basalts in the same area are evident, based on and a wider range and high of ($^{87}Sr/^{86}Sr$)i and the relatively low $\varepsilon Nd(t)$ values of the MAs (Fig. 8).

Discussion

Source materials

The experiments on natural, hydrous basalts at 1–4 GPa demonstrate that the high Mg contents of MAs cannot be produced by merely slab partial melting (Fig. 2; Rapp et al. 1999). In addition, the relatively low positive and wide range of $\varepsilon Nd(t)$ values, relatively high and wide range of ($^{87}Sr/^{86}Sr$)I ratios and the high concentrations of Cr, Ni and HREE suggest that juvenile crustal materials were involved in the source region of the MAs (Fig. 8).These juvenile materials were mainly composed of volcanic and volcaniclastic sediments coming from the forearc accretionary prism, they have not experienced strong multi-recycling weathered in crust and are characterized by low maturity with mantle geochemical signature. Moreover, the role of subducting oceanic slab as the main source material for the MAs from elsewhere, based on their high Sr and low *Y* concentrations and their low of Ti/Zr, Th/La and La/Yb ratios, which are obviously different from the normal island arc volcanic rocks, has been proposed (Yogodzinski et al. 1995; Drummond et al. 1996; Kelemen et al. 2003). On a Sr/Y versus Y diagram, however, the north Xinjiang MAs plot in the transition area between fields for adakites (or pure slab melts) and normal island arc andesite, dacite and rhyolite (ADR, Fig. 6). In addition, since heavy REEs (such as Yb) are compatible in garnet, the middle to heavy REE ratios $(Dy/Yb)_N$ in eclogite melts should be high (Kelemen et al. 2003). North Xinjiang MAs are chracterized by low $(Dy/Yb)_N$ (0.79–1.24) and relatively wide range of $(La/Yb)_N$(0.98–7.02) (Fig. 4) comparing with that of primitive mantle(Sun and McDonough 1989). The arrow in Fig. 4 shows the reaction of partial melts of MORB with upper

Table 3 Sr and Nd isotopic compositions of magnesian igneous rocks in north Xinjiang

Rock type	MAs							Magnesian dacite		
Location	Guozigou (1)	Road 312	North Weiya (1)	Alataoshan	Alataoshan	Saerbulake		Ashele		
Sample no	xt358	2079	2215	Xt26	wxt750	Sa-1	Sa-2	BB10-3	Az504-4	Az504-6	Az509-16
Sm	3.60	7.42	3.59	2.72	3.24	0.696	0.757	0.945	1.618	1.057	0.7871
Nd	15.79	60.1	16.3	12.43	14	2.611	2.522	3.399	5.692	3.649	2.448
$^{147}Sm/^{144}Nd$	0.1379	0.0746	0.1335	0.1325	0.1411	0.1614	0.1818	0.1681	0.172	0.1753	0.1945
$^{143}Nd/^{144}Nd$	0.512660	0.512564	0.512581	0.512678	0.512567	0.512918	0.512936	0.512905	0.512644	0.512643	0.512702
($\pm 2\sigma$)	14	12	10	6	12	13	13	9	10	11	10
$(^{143}Nd/^{144}Nd)_i$	0.51238	0.51255	0.51255	0.51244	0.51227	0.51252	0.51249	0.51250	0.51222	0.51221	0.51222
$\varepsilon_{Nd}(t)$	2.72	3.78	1.59	2.98	0.9	7.2	6.5	6.6	0.44	0.28	1.32
T_{2DM} (Ma)	764	707	869	711	1.220	485	563	528	920	933	916
Rb	23.36	163.0	16.7	42.61	20.8	30.21	22.7	28.48	10.58	9.54	5.96
Sr	591.6	488.0	543.0	502.6	265.0	130.7	304.58	242.2	100.4	98.17	24.79
$^{87}Rb/^{86}Sr$	0.1287	0.9683	0.0888	0.2453	0.2270	0.2311	0.0745	0.3402	0.3051	0.2816	0.6962
$^{87}Sr/^{86}Sr$	0.705524	0.707546	0.706532	0.704918	0.707544	0.707346	0.705049	0.707000	0.707575	0.707549	0.709462
($\pm 2\sigma$)	22	16	14	23	11	16	17	40	18	19	26
$(^{87}Sr/^{86}Sr)_i$	0.7050	0.7029	0.7061	0.7040	0.7065	0.7038	0.7039	0.7052	0.7059	0.7060	0.7057

World average boninite: $^{87}Sr/^{86}Sr = 0.70423$; $^{147}Sm/^{144}Nd = 0.51294$ Kelemen et al. (2003)

mantle peridotite (Kelemen et al. 2003). Both low $(La/Sm)_N$ ratios (1.41–4.06) and high and wide range $(Ba/Th)_N$ ratios (38–803.7) reveal the major contribution of subducted oceanic slab (Tatsumi 2006). Consequently, these features may suggest that the MAs are not pure slab melts, they are spatially and temporally associated with adakites in north Xinjiang (Wang et al. 2006; Niu et al. 2006a) and thus slab melts may have also been involved in their generation. These slab melts must have interacted with the mantle wedge to produce the north Xinjiang MAs. Finally, the obvious depletions of Nb, Ta and Ti, enrichments of LIL elements and relatively high and wide range of Ba/La ratios (Figs. 5 and 7) also reveal the involvement of subducted slab-derived fluids in the source materials. In summary, data suggest that the north Xinjiang MAs have a mutli-component source consisting of subducted oceanic slab, juvenile crustal materials coming from the accretionary prism, mantle wedge peridotite, and subducted slab-derived fluids.

Petrogenesis of MAs

In the 1990s, models of MAs genesis mainly invoked partial melting of harzburgitic or iherzolitic mineral assemblages under H_2O-saturated and H_2O-unsaturated conditions (Tatsumi 1981; Umino and Kushiro 1989; Kushiro 1972, 1974, 1975). However, more recent data on tectonic occurrence of MAs, their geochemical similarities with adakites and experiments on high-pressure melting of basalt have revealed that some arc magmas can be generated through partial melting of subducted oceanic crust under high geotherm and fluid-rich conditions (Kay 1978; Defant and Drummond 1990; Defant and Kepezhinskas 2001; Rapp et al. 1999; Sen and Dunn 1994). Moreover, results of experiments on the interaction of slab melts with mantle wedge peridotite (Green 1973, 1976; Fisk 1986; Kelemen et al.1990; Rapp et al. 1999; Prouteau et al. 1999) suggest that reaction of slab melts with mantle wedge peridotite is a reasonable mechanism for MA magma production. Tatsumi and Hanyu (2003) and Tatsumi (2006) modeled quantitatively other possible mechanisms for production of MA magmas such as through slab dehydration, partial melting of subducting slab and melt-solid reactions. Their modeling results suggest that slab melting and subsequent melt-mantle interaction reasonably reproduce the trace element characteristics of Setouchi MAs and sediment contribution is required for their Sr and Nd isotopic compositions.

Quantitative models of partial melting of NMORB, mixing of NMORB melts with mantle wedge peridotite and crystal-fractionation were carried out on the relationship between Sr/Y and Y (Fig. 6) and the $\varepsilon_{Nd}(t)$ versus $(^{87}Sr/^{86}Sr)_i$ (Fig. 8) in this paper. It is evident that about amount of 40% partial melt of NMORB (Fig. 6 curve 1)

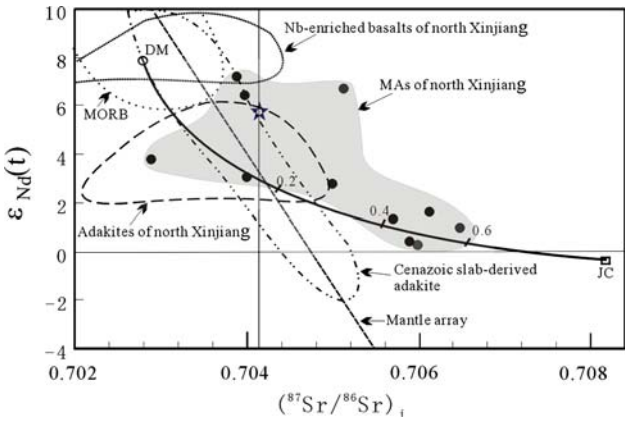

Fig. 8 Diagram of $\varepsilon Nd(t)$ versus $(^{87}Sr/^{86}Sr)I$ for the MAs in north Xinjiang. *DM* depleted mantle, *JC* juvenile crust; *Solid circle* and shaded area : north Xinjiang MAs; Star:world average boninite;The curve was drawn by means of mixing equation (Faure 1986) using the following endmember compositions:DM: $^{143}Nd/^{144}Nd$ 0.513114; $^{147}Sm/^{144}Nd$ 0.222; $^{87}Sr/^{86}Sr$ 0.703; $^{87}Rb/^{86}Sr$ 0.046; Nd 1.35 ppm, Sr 90 ppm (Data from McCulloch and Black 1984; Saunders et al., 1988); JC: $^{143}Nd/^{144}Nd$ 0.5125; $^{147}Sm/^{144}Nd$ 0.1540; $^{87}Sr/^{86}Sr$ 0.7086; $^{87}Rb/^{86}Sr$ 0.9167; Sm 2.8 ppm,Nd 11 ppm, Sr 348 ppm, Rb 11 ppm (Data from Allegre and Othman 1980; Tatsumi 2006; Rudnick and Gao 2003); $t = 320$ Ma

and subsequent reaction with the mantle wedge peridotite (OMW) is concord with the north Xinjiang MAs, the ratios of mantle wedge peridotite with the NMORB melts are about from 2:8 to 4:6(Fig. 6 curve 2), but the crystal-fractionation model is not fit to the north Xinjiang MAs (Fig. 6 curve 3). In the diagram of $\varepsilon_{Nd}(t)$ versus $(^{87}Sr/^{86}Sr)_i$ (Fig. 8), the one end member is DM representing the NMORB, the other one is juvenile crust (JC). The mixing calculations show that when the JC:DM ratios are from 2:8 to 4:6, the generated hybridized melts are better fitted the north Xinjiang MAs (Fig. 8, Faure 1986). On the other hand, fractional crystallization of a basaltic magma cannot result in the high concentrations of Cr, Ni and Mg of the MA magma (Polat and Kerrich 2001; Tatsumi et al. 2003; Tatsumi 2006; Streck et al. 2007). Additionally, Tatsumi (2006) stated that the basalt magma can yield the MAs through the process of assimilation and fractional crystallization (AFC) in terms of major element concentrations. However, such AFC processes cannot reproduce some trace element (K, Ba, Rb, Zr, Os, Re) and Sr-Nd–Pb isotopic characteristics of MAs.

Summary and conclusions

There are several factors that can account for the petrological and geochemical characteristics of MAs:

1. Multi-component source materials and complex petrogenesis

The source materials of MAs in north Xinjiang consist predominantly of melts from subducted oceanic slab with smaller contributions from sediments of the forearc prism and mantle wedge peridotite. The petrogenesis of MAs involves partial melting of the subducted oceanic crust, the subduction erosion of the sediments from the forearc prism and reaction of slab melts with mantle wedge peridotite (melt metasomatism) that had previously been metasomatized by slab-derived hydrous fluids. These feature scan account for the wide range of $(^{143}Nd/^{144}Nd)i$ ratios (0.512271–0.512554) and $(^{87}Sr/^{86}Sr)i$ ratios (0.7029–0.7065), the relatively low and wide range of $\varepsilon Nd(t) = +0.28$ to $+7.2$ and Nd model ages(T2DM) of 707–1,220 Ma. Some high $Mg^{\#}$ dacites may have formed by differentiation of HMA (Kelemen 1995).

2. High geothermal gradient and volatile-rich in MA source region

An inverted geothermal gradient is the essential for reaching the high temperature (> 1,000°C) of MA generation (Kelemen 1995). For example, high temperature (>950°C) basic granulite is associated closely with MAs in the Fuyun area (Li et al. 2004). Most experiments on MA petrogenesis in the presence of sufficient H_2O have proven the source region of MA is rich in volatiles (Tatsumi and Maruyama 1989).

3. Relatively low oxygen fugacities fO_2

V/Sc systematics in peridotites, mid-ocean ridge basalts and arc basalts may constrain the variation of $f\,O_2$ in the asthenosphere. The average V/Sc-inferred $f\,O_2$s for these rocks are remarkablely similar (–1.25 to +0.5 log units from the fayalite-magnetite-quartz (FMQ) buffer, Lee et al. 2003, 2005). The average V/Sc ratio of MAs in north Xinjiang is 5.96 and the respective average MgO = 5.22%. On a V/Sc versus MgO diagram, these rocks plot at about −1 log unit from the FMQ buffer. This is similar to that of average boninites (70 samples, V/Sc = 5.16, Kelemen et al. 2003) and lower than that of island arc ADR (473 samples,V/Sc = 6.51, Drummond et al. 1996;−0.6 log unit from FMQ, Lee et al. 2005) and Cenozoic average adakites (140 samples, V/Sc = 7.91, close to FMQ; Drummond et al. 1996) (Fig. 9). Differences in these average V/Sc ratios may relate to the involvement of Juvenile crust materials coming from the forearc accretionary prism to the source regions and petrogenesis of MAs in north Xinjiang (black line in Fig. 9).

4. Tectonic implications

Modern magmas with MA affinities have been erupted or intruded throughout Earth history but appear to be most common in two epochs: one is in Archean

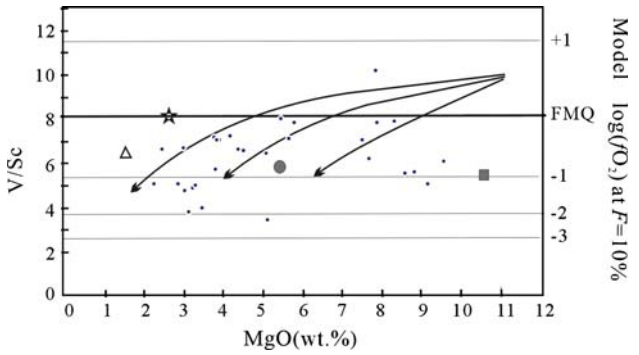

Fig. 9 Diagram of V/Sc versus MgO for the MAs in north Xinjiang (Lee et al. 2005, the data are from Table 2) Solid big *circle*; average MAs of north Xinjiang; Star: average of 140 Cenozoic adakite, Triangle : average of 473 ADR (Drummond et al. 1996; Solid square: average of 70 boninite (Kelemen et al. 2003). The curved black lines represent (from left to right) mixing lines between a lava having a hypothetically high primary V/Sc with estimated upper, average and lower continental crust (Lee et al. 2005)

greenstone belt, such as late-Archean Wawa greenstone belt in Canada, the other mainly in modern or Tertiary arc settings, such as the western Aleutian islands, Cape Vogel in Papua New Guinea, Setouchi volcanic belt and Bonin islands in Japan, Baja California in Mexico, and Isla Cook in south Chile. Their common features are the abnormally high geothermal gradients attributed to the high heat flow and rapid mantle convection or ridge-trench collision in Archean [(Defant and Drummond 1990; Polat et al. 1998; Polat and Kerrich 1999, 2001); and oblique flat subduction of young and hot oceanic lithosphere in Cenozoic (Tatsumi and Maruyama 1989; Defant and Drummond 1990; Kelemen 1995). These unusual and special tectonic settings are likely to play an important role in MA production. Late Paleozoic tectonic settings and final amalgamation time of the north Xinjiang remain the subject of debate. Such as for the amalgamation time there are: Devonian-Carboniferous (Han et al. 1997); Permian (Li et al. 2005; Xiao et al. 2004; Cooks and Tosvik 2007); end Permian-Triassic (Xiao WJ Windley et al. 2008 in the same issue); Triassic (Briggs et al. 2007). Based on the above observations, it is possible that the co-existence of MAs, adakites, niobium-enriched basalt and mafic-ultramafic igneous rocks in north Xinjiang during the late Paleozoic is due to a high geothermal gradient and heat flow, which may further imply the existence of an asthenosphere window that resulted from slab break off or ridge subduction (Fig. 1 a, b). This tectonic setting is similar to that found in the Aleutian islands or Baja California (Kelemen 1995; Rogers and Saunderst 1989) and reasonable deduced there were subduction-related settings during the Devinian-Carboniferous in north Xinjiang region.

5. Possible role of subduction erosion

Subduction erosion has been very important along the Chilean/Agentine Andean margin (von Huene and Scholl 1993). It is one of three distinct processes that transfer crustal mass to the mantle at convergent margins (Kay and Kay 2002). Subduction erosion is episodic, correlating with changes in plate subduction direction or rate, or with flattening or steeping of slab dip (Kay and Kay 2002). Where this process brings juvenile materials from forearc prism down with the subducting oceanic slab to high temperature regions such as an asthenosphere window, the sediments will melt together with the slab to form MA magmas.

6. Associated mineralization

Massive mineralizaios of Cu, Au and Zn(Pb) are closely temporally and spatially associated with the MAs in north Xinjiang. Many studies suggest the continental growth is very evident during Phaneozoic, particular the Late Paleozoic in north Xinjiang. This is evidenced from the widespread of the mafic-ultromafic igneous rocks, MAs and associated adakites and Nb-enriched basalts, and alkali-rich igneous rocks (Sengor et al. 1993; Zhao et al. 1993, 1996, 2000, 2006a, b, 2007; Han et al. 1997, 2006; Jahn et al. 2000, 2004). Nearly half of the gigantic Central Asia orogenic belt (CAOB) was derived from the mantle by arc accretion (Sengor et al. 1993). The MAs were the important products of the continental growth, their specific tectonic settings, such as ridge-trench collision and asthenosphere window, high geothermal gradient, slab melt-mantle interaction(melt metasomatism) and volatile-rich in MAs source and petrogenesis process would provide sufficient ore-forming materials (Cu, Au, Zn, Pb) and suitable conditions for the massive mineralization of Cu, Au and Zn, Pb, such as the decomposition of metallic sulfides and subsequent transportation into the MAs magma.

In summary, results of our investigation suggest the following:

1. Late Paleozoic MAs are widespread in north Xinjiang with a clear younging trend from north to south (from Devonian to Carboniferous).
2. The MAs span a range of SiO_2 53–65% with TiO_2 <1% and are characterized by $Mg^{\#}$ ≥50, high contents of compatible elements Cr and Ni and relative depletions of high field strength elements Nb and Ta. Low total REE contents and flat chondrite-normalized REE patterns with weak or no depletion of Eu anomalies are characteristics of these MAs. The MAs

also possess a wide range of ($^{143}Nd/^{144}Nd$)i and ($^{87}Sr/^{86}Sr)_i$ ratios, relatively low and wide range of $\varepsilon Nd(t)$ and Nd model ages.

3. Petrographic and geochemical evidences indicate that the MAs from north Xinjiang have involved multi-component source materials, a multi-stage petrogenesis, high geothermal gradient and high volatile contents combined with relatively low oxygen fugacities fO_2 in their source region. Specific tectonic settings, such as ridge-trench collision, asthenosphere window that may have resulted from slab break off or ridge subduction and subduction erosion, may be further involved in the generation of MAs in north Xinjiang.

Acknowledgments This study was jointly supported by National Basic Research Program of China (2007CB411303;),and the National Natural Science Foundation of China (No 40721063 and 40673037). We thank Dr. Derek Wyman for his helpful suggestions and comments on the manuscript The constructive reviews from Dr. P R Castillo and other anonymous reviewer have substantially improved the manuscript. The topic editor Dr. Wenjiao Xiao is much appreciated for his beneficial suggestions.

References

Adam J, Green TH, Sie SH (1993) Proton microprobe determined partitioning of Rb, Sr, Ba, Y, Zr, Nb, and Ta between experimentally produced amphyboles and silicate melts with variable F content. Chem Geol 109:29–49

Allegre CJ, Minster JF (1977) Quantitative models of trace element behavior in magmatic processes. Earth Planet Sci Lett 38:1–25

Allegre CJ, Othman DB (1980) Nd–Sr isotopic relationship in granitoid rocks and continental crust development: a chemical approach to orogenesis. Nature 286:335–341

Briggs SM, Yin A, Manning CE, Chen ZL, Wang XF, Grove M (2007) Late Paleozoic tectonic history of the Ertix Fault in the Chinese Altai and its implications for the development of the Central Asia Orogenic System. Geol Soc Am Bull 119:944–960

Chen YC, Ye QT, Feng J, Mou CL, Zhou LR, Wang QM, Huang GZ, Zhuang DZ, Ren BS (1996) Ore-forming conditions and metallogenic prognosis of the Ashele copper–zinc metallogenic belt, Xinjiang China. Geological Publishing House, Beijing, pp 8–9 (in Chinese with English abstract)

Chen JF, Zhou TX, Xie Z, Zhang X, Guo XS (2000) Formation of positive ε Nd (T) granitoids from the Alataw Mountains, Xinjiang, China by mixing and fractional crystallization: implication for Phanerozoic crustal growth. Tectonophysics 328:53–67

Chen YC, Liu DQ, Wang DH, Tang YL, Zhou RH, Chen ZY (2004) Discovery and geological significance of picritic rocks in north Junggar, Xinjiang. Geol Bull China 23:1059–1065 (in Chinese with English abstract)

Chen FW, Li HQ, Chen YC, Wang JL, Liu DQ, Zhou RH (2005) Zircon SHRIMP U-Pb dating and its geological significance of mineralization in Tuwu-Yandong porphyry copper mine, east Tianshan mountain. Acta Geol Sin 79:256–261

Crawford AJ, Falloon TJ, Green TH (1989) Classification, petrogenesis and tectonic setting of boninites. In: Crawford (ed) Unwin Hyman, Boninites pp 1–49

Cooks LRM, Tosvik TH (2007) Sibiria, the wandering northern terrane, and its changing geography through the Paleozoic. Earth Sci Rev 82:29–74

Defant MJ, Drummond MS (1990) Derivation of some modern arc magmas by young subducted lithosphere. Nature 347:662–665

Defant MJ, Drummond MS (1993) Mount St. Helens: potential example of the partial melting of subducted lithosphere in a volcanic arc. Geology 21:547–550

Defant MJ, Kepezhinskas P (2001) Evidence suggests slab melting in arc magmas. EOS 82:62–69

Drummond MS, Defant MJ, Kepezhinskas PK (1996) The petrogenesis of slab derived trondhjemite–tonalite-dacite/adakite magmas. Trans R Soc Edinb Earth Sci 87:205–216

Faure G (1986) Principles of isotope geology, 2nd edn. Wiley, New York, pp 142–144

Fisk MR (1986) Basalt magma interaction with harzburgite and the formation of high-magnesian andesites. Geophys Res Lett 13:467–470

Gao S, Zhang BR, Gu X, Xie X, Gao C, Guo X (1995) Siliurian-Devonian provenance changes of South Qinling basin: implications for accretion of the Yangtze (South China) to the North China Craton. Tectonophysics 250:183–197

Gao J, Long LL, Qian Q, Huang DZ, Su W, Klemd R (2006) South Tianshan: a late Paleozoic or Triassic orogen? Acta Petrol Sin 22:1049–1061 (in Chinese with English abstract)

Green DH (1973) Experimental melting studies on a model upper mantle composition at high pressure under water-saturated conditions. Earth Planet Sci Lett 19:37–53

Green DH (1976) Experimental testing of "equilibrium" partial melting of peridotite under water-saturated, high pressure conditions. Can Mineral 14:255–268

Green TH (1994) Experimental studies of trace-element partitioning applicable to igneous petrogenesis -Sedona 16 years later. Chemical Geol 117:1–36

Green TH, Ringwood AE (1968) Genesis of the calk-alkaline igneous rock suit. Contrib Mineral Petrol 18:105–162

Green TH, Sie SH, Ryan CG, Cousens DR (1989) Proton microprobe-determined partitioning of Nb, Ta, Zr, Sr and Y between garnet, clinopyroxene and basaltic magma at high pressure and temperature. Chem Geol 74:201–216

Grove TL, Parman SW, Bowring SA, Price RC, Baker MB (2002) The role of H_2O-rich fluid component in the generation of primitive basaltic andesites and andesites from the Mt. Shadta region, N California. Contrib Miner Petrol 142:375–396

Han BF, Wang SG, Jahn BM, Hong DW, Kagami H, Sun YL (1997) Depleted-mantle magma source for the Ulungur River A-type granites from north Xinjiang, China: geochemistry and Nd-Sr isotopic evidence, and implication for Phanerozoic crustal growth. Chem Geol 138:135–159

Han BF, Ji JQ, Song B, Chen LH, Zhang L (2006) Late Paleozoic vertical growth of continental crust around the Junggar Basin, Xinjiang, China (part I). Acta Petrol Sin 22:1077–1086 (in Chinese with English abstract)

Jahn BM, Griffin WL, Windley BF (2000) Continental growth in the Phanerozoic: evidence from central Asia. Tectonophysics 328:1–227

Jahn BM, Windley B, Natalin B, Dobretsov N (2004) Phanerozoic continental growth in central Asia. J Asian Earth Sci 23:599–603

Jenner GA (1981) Geochemistry of high-Mg andesites from Cape Vogel, Papua New Guinea. Chem Geol 33:307–332

Jenner GA, Foley SF, Jackson SE, Green TH, Fryer BJ, Longerich HP (1993) Determination of partition coefficients for trace elements in high pressure-temperature experimental run products by laser ablation microprobe-inductively coupled plasma mass spectrometry (LAM-ICP-MS). Geochim Cosmochim Acta 57:5099–5103

Kay RW (1978) Aleutian magnesian andesites: melts from subducted Pacific ocean crust. J Volcanol Geotherm Res 4:117–132

Kay RW, Kay SM (2002) Andean andesites: three ways to make them. Acta Petrol Sin 18:303–311

Kelemen PB (1995) Genesis of high $Mg^{\#}$ andesites and the continental crust. Contrib Mineral Petrol 120:1–19

Kelemen PB, Joyce DB, Webster JD, Holloway JR (1990) Reaction between ultramafic wall rock and fractionating basaltic magma: pert II, experimental investigation of reaction between olivine tholeiite and harzburgite at 1,150 and 1050°C and 5 kbar. J Petrol 31:99–134

Kelemen PB, Hanghoj K, Greene AR (2003) One view of the geochemistry of subduction-related magmatic arcs, with an emphosis on primitive andesite and lower crust. In: Holland HD, Turekian KK (eds) Treatise on geochemistry, vol 3. Elsevier, Amsterdam, pp 593–660

Kennedy AK, Lofgren GE, Wasserburg GJ (1993) An experimental study of trace element partitioning between olivine, orthopyroxene and melt in chondrules: equilibrium values and kinetic effects. Earth Planet Sci Lett 115:177–195

Kikuchi Y (1889) On pyroxenic components in certain volcanic rocks from Bonin Island. J Coll Sci Imp Univer Japan 3:67–89

Kushiro I (1972) Effect of water on the composition of magmas formed at high pressures. J Petrol 13:311–334

Kushiro I (1974) Melting of upper mantle and possible generation of andesitic magma: an approch from synthetic systems. Earth Planet Sci Lett 22:294–299

Kushiro I (1975) On the nature of silicate melts and its significance in magma genesis:regulirities in the shift of the liquids boundaries involving olivine, pyroxene, and silica minerals. Am J Sci 275:411–431

Le Maitre RW (ed) (2002) Igneous rocks, a classification and glossary of terms, Cambridge University Press, Cambridge, pp 34–35

Lee C-T, Brandon AD, Norman M (2003) Vanadium in peridotite as a proxy for paleo-fO_2 during partial melting:prospects, limitatios, and implications. Geochim Cosmochim Acta 67:3045–3064

Lee C-TA, Leeman WP, Canil D, Li Z-X (2005) Similar V/Sc systematics in MORB and arc basalts: implications for the oxygen fugacities of their mantle source regions. J Petrol 46:2313–2336

Li HQ, Xie CF, Chang HL et al (1998) Study on metallogenetic chronology of nonferrous and precious metallic ore deposits in North Xinjiang, China. Geological Publishing House, Beijing, pp 107–127 (in Chinese with English abstract)

Li YJ, Sun LD, Wu HR, Wang GL, Yang CS, Peng GX (2005) Permo-Carbonifereous radiolaria from the Wupatarkan Group, west terminal of Chinese South Tianshan. Chin J Geol 40:220–226 (in Chinese with English abstract)

Li JY, Wang KZ, Sun GH, Mo SG, Li WQ, Yang TN, Gao LM (2006) Paleozoic active margin slices in the southern Turfan-Hami basin:geological records of subduction of the Paleo-Asian Ocean plate in central Asian regions. Acta Petrol Sin 22:1087–1102 (in Chinese with English abstract)

Li ZL, Santosh M, Chen HL, Yang SF (2004) First report of high-T spinel-garnet granulite from the Altay orogenic belt, NW China. Gondwana Research (Supp) 7:1335–1336

Liang XR, Wei GJ, Li XH, Liu Y (2003) Precise measurement of $^{143}Nd/^{144}Nd$ and Sm/Nd ratios using multiple-collectors inductively coupled plasma-mass spectrometer(MC-ICPMS). Geichimica 32:91–96 (in Chinese with English abstract)

Liu DQ, Tong YL, Zhou RH (1993) Devonian intraoceanic arc and boninite in north Junggar, Xinjiang. Geology 11:1–12 (in Chinese with English abstract)

Liu Y, Liu HC, Li XH (1996) Simultaneous and precise determinination of 40 trace elements in rock samples by ICP-MS. Geochimica 25:552–558

Liu DQ, Chen YC, Wang DH, Tang YL, Zhou RH, Wang JL, Li HQ, Chen FW (2003) A discussion on problems related to mineralization of Tuwu-Yandong Cu–Mo orefield in Hami, Xinjiang. Miner Dep 22:334–344 (in Chinese with English abstract)

McCarro JJ, Smellie JL (1998) Tectonic implications of fore-arc magmatism and generation of high-magnesian andesites: Alexander Island, Antarctica. J Geol Soc London 155:269–280

Nagao T, Kakubuchi S, Shiraki K (1997) Quantitative major and trace element analyses of rock by X-ray fluorescence spectrometry (Rigaku/RIX3000). Report of center for Instrumental Analysis. Yamaguchi University, vol 5, pp 10–15

Niu HC, Sato H, Zhang HX, Ito J, Yu XY, Nagao T, Terada K, Zhang Q (2006a) Juxtaposition of adakite, boninite, high-TiO_2 and low-TiO_2 basalts in the Devonian southern Altay, Xinjiang, NW China. J Asian Earth Sci 28:439–456

Niu HC, Yu XY, Xu JF, Shan Q, Chen FR, Zhang HX, Zheng ZP (2006b) Late Paleozoic volcanism and associated metallogenesis in the Altay area, Xinjiang, China. Geological Publishing House, Beijing, pp 8–68 (in Chinese with English abstract)

Polat A, Kerrich R, Wyman DA (1998) The late Archean Schreiber-Hemlo and White River-Dayohessarh greenstone belts, Superior Province:collages of oceanic plateaus, oceanic arcs and subducion-accretion complexes. Tectonophysics 294:295–326

Polat A, Kerrich R (1999) Formation of an Archean tectonic melange in the Schreiber-Hemlo greenstone belt, Superior Province, Canada: implications for Archean subduction-accretion process. Tectonics 18:733–755

Polat A, Kerrich R (2001) Magnesian andesites, Nb-enriched basalt-andesites, and adakites from late-Archean 2.7 Ga Wawa greenstone belts, Superior Province, Canada: implications for late Archean subduction zone petrogenetic processes. Contrib Mineral Petrol 141:36–52

Prouteau G, Scaillet B, Pichacent M, Maury RC (1999) Fluid-present melting of oceanic crust in subduction zones. Geology 27:1111–1114

Rapp RP, Shimizu MD, Morman GS (1999) Reaction between slab-derived melts and peridotite in the mantle wedge:experimental constraints at 3.8 Gpa. Chem Geol 160:333–356

Rogers G, Saunderst AD (1989) Magnesian andesites from Mexico,Chile and the Aleutian islands: implications for magmatism associated with ridge-trench collision. In: Crawford (ed) Boninites, Unwin Hyman, London, pp 417–442

Rudnick RL, Fountain DM (1995) Nature and composition of the continental crust: a lower crustal perspective. Rev Geophys 33:267–309

Saunders AD, Norry MJ, Tarney J (1988) Origin of MORB and chemically depleted mantle reservoirs: trace element constrants. J Petrol (Special lithosphere issue) 425–445

Sen C, Dunn T (1994) Dehydration melting of a basaltic composition amphibolite at 1.5 and 2.0 GPa: implication for the origin of adakites. Contrib Mineral Petrol 117:394–409

Sengor AMC, Natal'in BA, Burtman US (1993) Evolution of the Altaid tectonic collage and Paleozoic crustal growth in Eurasia. Nature 364:209–304

Streck MJ, Leeman WP, Chesly J (2007) High-magnesian andesite from Mount Shasta: A product of magma mixing and contamination, not a primitive mantle melt. Geology 35:351–354

Sun SS, McDonough WF (1989) Chemical and isotopic systematics of ocanic basalts:implications for mantle composition and processes. Geological Society of London. Special Publication 42:313–345

Tatsumi Y (1981) Melting experiments on a high-magnesian andesites. Earth Planet Sci Lett 54:357–365

Tatsumi Y, Maruyama S (1989) Boninites and high-Mg andesites: tectonics and petrogenesis. In: Crawford (ed) Boninites. Unwin Hyman, London, pp 50–71

Tatsumi Y, Hanyu T (2003) Geochemical modeling of dehydration and partial melting of subducting lithosphere: twards a comprehensive understanding of high-Mg andesite formation in the Setouchi volcanic belt, SW Japan. Geochem Geophy Geosyst 4, 1081, doi:10.29/2003GC000530

Tatsumi Y, Shukuho H, Sato K, Shibata T, Yoshikawa M (2003) The petrology and geochemistry of high-Mg andesites at the western tip of the Setouchi volcanic belt, SW Japan. J Petrol 44:1561–1578

Tatsumi Y (2006) High-Mg andesites in the Setouchi volcanic belt, southwester Japan: analogy to Archean magmatism and continental crust formation? Annu Rev Earth Planet Sci 34:467–499

Taylor SR, McLennan SM (1995) The geochemical evolution of continental crust. Rev Geophys 33:241–265

Umino S, Kushiro I (1989) Experimental studies on boninite pertrogenesis. In: Crawford AJ (ed) Boninite. Unwin Hyman, London, pp 89–112

von Huene R, Scholl DW (1993) The return of sialic material to the mantal indicated by terrigenous material subducted at convergent margions. Tectonophysics 219:163–175

Wang Q, Zhao ZH, Xu JF, Wyman DA, Xiong XL, Zi F, Bai ZH (2006) Carboniferous adakite-high-Mg andesite–Nb-enriched basaltic rock suites in the Northern Tianshan area:Implications for Phanerozoic crustal growth in the Central Asian Orogenic Belt and Cu–Au mineralization. Acta Petrol Sin 22:11–32 (in Chinese with English abstract)

Woodhead JD, Hergt JM, Davidson JP, Eggins SM (2001) Hafnium isotope evidence for "conservation" element mobility during subduction zone processes. Earth Planet Sci Lett 192:331–346

Warner RD (1973) Liquidus relations in the system CaO–MgO–SiO_2–H2O at 10 KB PH_2O and their petrologic significance. Am J Sci 273:925–946

Xiao XC, Tang YQ, Fen YM, Zhu BQ, Li JY, Zhao M (1992) Tectonic evolution of northern Xinjiang and its adjacent region. Geological Publishing House, Beijing, pp 1–180 (in Chinese with English abstract)

Xiao WJ, Windley BF, Bardach G, Sun S, Li J, Qin K, Wang Z (2004) Paleozoic accretion and convergent tectonics of the southern Altaids: implications for the lateral growth of Central Asia. J Geol Soc London 161:339–342

Xiao WJ, Han CM, Yuan C, Chen HL, Sun M, Lin SF, Li ZL, Mao QG, Zhang JE, Sun S, Li JL (2006) Unique Carboniferous-Permian tectonic-metallogenic framework of northern Xinjiang (NW China): constrains for thetectonic of the southern Paleo-asian domain. Acta Petrol Sin 22:1062–1076 (in Chinese with English abstract)

Xiao WJ Windley BF, Han CM, Huang BC, Yuan C, Chen HL, Sun M,Li JL (2008) End-Permian to Trassic termination of the southern Altaids: implications for the Phaneozoic continental growth and massive metallogeny of Central Asia. Int J Earth Sciences (this issue)

Xu XY, Ma ZP, Xia LQ, Li M, Xia ZC, Wang LS (2005) Accurate dating of Bayingou ophiolite in northern Tianshan mountains and its tectonic significance. J Earth Sci Environ 27:17–20 (in Chinese with English abstract)

Xu XY, Li XM, Ma ZP, Xia LQ, Xia ZC, Peng SX (2006) LA-ICPMS zircon U–Pb dating of gabbro from the Bayingou ophiolite in thenorthern Tianshan Mountan. Acta Geologica Sinica 80:1168–1175 (in Chinese with English abstract)

Yogodzinski GM, Kay RW, Volynets ON, Koloskov AV, Kay SM (1995) Magnesian andesite in the western Aleutian Komandorsky region: implications for slab melting and processes in the mantle wedge. Geol Soc Am Bull 107:505–519

Zhai W, Sun XM, Gao J, He XP, Liang JL, Huang LC, Wu YL (2006) SHRIMP dating of zircon from volcanic host rocks of Dahalajunshan formation in Axi gold deposit, Xinjiang, China, and its geological implications. Acta Petrol Sin 22:1399–1404

Zhang HF, Sun M, Zhou XH (2002) Mesozoic lithosphere destruction beneath the North China: evidence from major-, trace-element and Sr–Nd–Pb isotope studies of Fangcheng basalts. Contrib Mineral Petrol 144:241–253

Zhang HX, Niu HC, Yu XY, Sato H, Ito J, Shan Q (2003) Geochemcal characteristics of the Shaerbulake boninites and their tectonic significance, Fuyun County, northern Xinjiang, China. Geochimica 32:155–160 (in Chinese with English abstract)

Zhang ZC, Yan SH, Chen BL, Zhou G, He YS, Cai FM, He LX (2005) Middle Devonian picrites of South margin of Altay orogenic belt and implications for tectonic setting and petrogenesis. Earth Sci J China Univ Geosci 30:289–296 (in Chinese with English abstract)

Zhao ZH, Wang ZG, Zou TR, Masuda A (1993) The REE, isotopic composition of O, Pb, Sr and Nd and diageneticmodel of granitoids in Altay region. In :Tu G (ed) New improvement of solid geosciences in northern Xinjian. Science Press, Beijing, pp 239–266 (in Chinese)

Zhao ZH, Wang ZG, Zou TR, Masuda A (1996) Study on petrogenesis of alkali-rich intrusive rocks of Ulungur, Xinjiang. Geochimica 25:205–220 (in Chinese with English abstract)

Zhao ZH, Bai ZH, Xiong XL, Mei HJ, Wang YX (2000) Geochemistry of alkalirich igneous rocks of northern Xinjiang and its implications for geodynamics. Acta Geol Sin 74:321–328

Zhao ZH, Bai ZH, Xiong XL, Mei HJ (2006a) The alkali-rich igneous rocks and related mineralization in North Xinjiang, China. Geological Publishing House, Beijing, pp 12–148 (in Chinese with English abstract)

Zhao ZH, Wang Q, Xiong XL, Zhang HX, Niu HC, Xu JF, Bai ZH, Qiao YL (2006b) Two types of adakites innorth Xinjiang, China. Acta Petrologica Sinica 22:1249–1265 (in Chinese with English abstract)

Zhao ZH, Xiong XL, Wang Q, Wyman DA, Bao ZW, Bai ZH, QiaoYL (2007) Underplating- related adakites in Xinjiang Tianshan. Lithos doi:10.1016/j.Lithos.2007.06.008